WIND ENERGY
Wind Energ. (2011)
Published online in Wiley Online Library (wileyonlinelibrary.com). DOI: 10.1002/we.517

RESEARCH ARTICLE

Production of the Finnish Wind Atlas

Bengt Tammelin[1], Timo Vihma[1], Evgeny Atlaskin[1], Jake Badger[2], Carl Fortelius[1], Hilppa Gregow[1], Matti Horttanainen[1], Reijo Hyvönen[1], Juha Kilpinen[1], Jenni Latikka[1], Karoliina Ljungberg[1], Niels Gylling Mortensen[2], Sami Niemelä[1], Kimmo Ruosteenoja[1], Kirsti Salonen[1], Irene Suomi[1] and Ari Venäläinen[1]

[1] Finnish Meteorological Institute, Helsinki, Finland
[2] Risø DTU National Laboratory of Sustainable Energy, Denmark

ABSTRACT

The Finnish Wind Atlas was prepared applying the mesoscale model AROME with 2.5 km horizontal resolution and the diagnostic downscaling method Wind Atlas Analysis and Application Programme (WAsP) with 250 m resolution. The latter was applied for areas most favourable for wind power production: a 30 km wide coastal/offshore zone, highlands, large lakes and large fields. The methodology included several novel aspects: (i) a climatologically representative period of real 48 months during 1989–2007 was simulated with the mesoscale model; (ii) in addition, the windiest and calmest months were simulated; (iii) the results were calculated separately for each month and for sectors 30° wide; (iv) the WAsP calculations were based on the mesoscale model outputs; (v) in addition to point measurements, also radar wind data were applied for the validation of the mesoscale model results; (vi) the parameterization method for gust factor was extended to be applicable at higher altitudes; and (vii) the dissemination of the Wind Atlas was based on new technical solutions. The AROME results were calculated for the heights of 50, 75, 100, 125, 150, 200, 300 and 400 m, and the WAsP results for the heights of 50, 75, 100, 125 and 150 m. In addition to the wind speed, the results included the values of the Weibull distribution parameters, the gust factor, wind power content and the potential power production, which was calculated for three turbine sizes. The Wind Atlas data are available for each grid point and can be downloaded free of charge from dynamic maps at www.windatlas.fi. Copyright © 2011 John Wiley & Sons, Ltd.

KEYWORDS
wind atlas; wind resource mapping; mesoscale modelling; wind climate; atmospheric boundary layer; Finland

Correspondence
Timo Vihma, Finnish Meteorological Institute, Helsinki, Finland.
E-mail: timo.vihma@fmi.fi

Received 22 November 2010; Revised 10 June 2011; Accepted 17 August 2011

1. INTRODUCTION

Production of a new state-of-the-art Wind Atlas for Finland is expected to help the exploitation of wind energy resources for electricity production. Up to the end of 2009, the amount of wind energy capacity installed in Finland was only 147 MW (www.vtt.fi/ windenergystatistics). In the governmental development plan for renewable energy, the target is to have 2000–2500 MW of installed wind power by 2020. A feed in law came in force in 2011 guaranteeing a fixed price for electricity production, which strongly increased the interest in wind energy. Accordingly, identification and searching for potential sites for wind farms is a current issue in Finland.

The previous national Wind Atlas for Finland was produced in 1991.[1] It was based on use of the Wind Atlas Analysis and Application Programme (WAsP[2]) and wind data from 57 weather stations, using a methodology slightly modified from that in the European Wind Atlas.[3] The Finnish atlas from 1991 intended to present the long-term wind climate in the whole country, but the number of observations available was limited. At that time, the number of offshore and coastal weather stations was very low, whereas no wind measurements were available from the fjelds (barren, low mountains in northern Finland). Hence, the representativeness of the wind atlas for these areas, which actually have the highest wind energy potential, was not good. Furthermore, the results were only presented for the whole year without seasonal separation.

Accordingly, a strong need arose for a more accurate wind atlas. In Finland, the size of the country, its complex terrain and large seasonal differences generate strong demands for a wind atlas. The complexity of the terrain is not so much related to orography but to the complex shape of the almost flat coastline and archipelago, which generates a need for very high spatial resolution. Further, the differences in wind conditions between seasons are particularly large because in winter, the sea and lakes are frozen and the ground is covered by snow, which changes the surface roughness and stabilizes the atmospheric boundary layer (ABL). Stable stratification favours the generation of low-level jets.[4] In winter, wind power plants are also subject to ice accretion. The production of a new Wind Atlas for Finland has also been motivated by the need to evaluate the possible effects of climate change on wind conditions. In 2008, the Ministry of Labour and Economics released an international tender for production of the new Finnish Wind Atlas. The tender was won by the Finnish Meteorological Institute (FMI), with Risø DTU and Vaisala Ltd as subcontractors. The project started 1 June 2008, and the wind atlas was released 25 November 2009 (www.windatlas.fi).

Many national wind atlases have recently been produced applying numerical weather prediction (NWP) models. In an ideal approach, all possible weather conditions should be simulated. Experiments with NWP models require, however, many computer resources. Hence, in recent wind atlas projects, the number of cases simulated has usually been limited to a few hundred, and the results have been weighted applying various statistical methods to represent the annual mean wind conditions. The Swedish Wind Atlas was produced applying a mesoscale model.[5] The model was forced by various geostrophic wind fields, and the seasonal variations in temperature and humidity were also taken into account. The model results were weighted on the basis of the climatological distribution of geostrophic winds based on pressure observations and the National Centers for Environmental Prediction/National Center for Atmospheric Research (NCEP/NCAR) reanalysis fields on the altitude of the 850 hPa pressure level. Also, the Portuguese[6] and Spanish[7] Wind Atlases were produced by mesoscale models. Long-term wind observations were used to weight the mesoscale model results calculated for selected geostrophic flow fields.

It has been more common to produce wind atlases applying a combination of mesoscale and microscale models. In Denmark and Faroe Islands[8] and in Egypt,[9] the mesoscale model Karlsruhe Atmospheric Mesoscale Model was applied together with WAsP. The simulated weather situations were selected on the basis of the NCEP/NCAR reanalysis data, and the average wind climate was obtained by weighting the Karlsruhe Atmospheric Mesoscale Model results on the basis of the frequency of occurrence of various large-scale atmospheric forcing conditions. The Irish Wind Atlas[10] was based on the mesoscale model Mesoscale Atmospheric Simulation System, the mass-consistent model Windmap and the NCEP/NCAR reanalysis data. In Italy,[11] the wind flow model WINDS was applied with wind observations and 10 years of geostrophic wind data based on the European Centre for Medium-Range Weather Forecasts reanalysis. The Norwegian Wind Atlas differs from other wind atlases because instead of geostrophic wind data and a mesoscale model, solely the computational fluid dynamic model WindSim was applied with long-term wind observations (http://windsim.com/wind_energy/wind_atlas/).

In this paper, we describe the production methodology of the Finnish Wind Atlas and present some examples of the results. Our modelling strategy (Section 2) was based on application of two models: the mesoscale model AROME with 2.5 km horizontal resolution and the diagnostic downscaling method WAsP with 250 m horizontal resolution. Our approach differs significantly from those previously applied in the production of national wind atlases: we simulated a much larger number of real weather conditions than previously carried out. In the wind atlas, we also present variables based on post-processing of the model results, which is described in Section 3. In Section 4, we summarize the validation of AROME and WAsP, including a novel application of radar winds, and in Section 5, we evaluate climatological aspects of wind conditions in Finland. Examples of the results of the wind atlas are presented in Section 6, and conclusions are drawn in Section 7.

2. MODELLING STRATEGY

2.1. Selection of simulation period

The Finnish Wind Atlas was requested to represent the present wind climate. Hence, we first studied the wind speeds at the 850 hPa pressure level utilizing the ERA-40 and ERA-Interim reanalysis of the European Centre for Medium-Range Weather Forecasts for the period of 1958–2007. In the total period of 1958–2007, an increasing trend was found in the 850 hPa wind speed over Finland, but in the subperiod of 1989–2007, covered by ERA Interim, there was no statistically significant trend. Hence, an objective was set that the Finnish Wind Atlas should as well as possible represent the period of 1989–2007. In lieu of time and computing power for a 19-year-long AROME simulation, we decided to simulate a representative 48-month-long reference period. We selected the period so that the wind conditions of each month are represented by winds of that month in four selected years. The selection was made on the basis of the ERA-Interim 850 hPa level data on wind speed and direction.

The number of possibilities to select 4 years among 19 years is 5430 (when the same year is allowed to be selected more than once). The selection between these alternatives was made on the basis of following criteria:

(a) The Weibull distribution of wind speed should be as representative as possible for the period 1989–2007.
(b) The distribution of wind directions should be as representative as possible.
(c) The Weibull distribution of wind speed should be as representative as possible in the 12 wind direction sectors (each 30° wide).

The following calculations were made separately for each month at the 850 hPa pressure level at nine locations: two in northern Finland, three at the coast of the Gulf of Bothnia, two at the coast of the Gulf of Finland and two in inland central Finland. From the 5430 possible combinations of years, the minimum values were searched for parameters R_S and R_D.

$$R_S = 6|k_i - \overline{k}| + |A_i - \overline{A}| \tag{1}$$

R_S measures the representativeness with respect to aspect (a): i refers to the Weibull parameter value in a combination of 4 years, and the overbar refers to the parameter value in the 19 year data set. The factor 6 is applied to make the deviations of A and k equally important for R_S.

$$R_D = \sum_{D=1}^{12} |V_i^D - \overline{V^D}| + |P_i^D - \overline{P^D}| \tag{2}$$

R_D measures the representativeness with respect to aspects (b) and (c). D is the wind direction sector: $D_1 = 0$–30°, $D_2 = 30$–60°, and so on. V is the wind speed, and P is the percentage of cases in each wind direction sector. The final parameter to be minimized is

$$R = 20\, R_S + R_D \tag{3}$$

where the factor 20 makes $R_S + R_D$ equally weighted. Finally, the combination of years to be simulated is the one that minimizes the sum of R over the nine locations.

In addition, 12 individual months were selected to represent the most windy hypothetical year (composed of the most windy January, February, and so on, in the period 1989–2007) and analogously the least windy hypothetical year. The months selected for the AROME simulations are shown in Table I.

2.2. Use of the NWP models

The NWP models HIRLAM and AROME were applied to produce the wind atlas. HIRLAM[12] is the main tool of FMI for synoptic-scale NWP; it provided initial and boundary conditions for AROME, which is described in Appendix A. The HIRLAM and AROME runs were conducted in double-nesting manner following the operational practice at FMI (Figure 1). All the wind atlas periods (Table I) were simulated in 6 hour sequences, storing the atmospheric state after 3 and 6 h of simulation. The 3-hourly output was chosen to adequately capture the diurnal cycle of the wind field. AROME used a 2.5 km horizontal grid spacing and 40 hybrid terrain-following levels in the vertical, defined in terms of pressure, of which eight levels were located in the lowest 1000 m (approximate heights above the model surface: 30, 100, 185, 280, 390, 520, 665 and 830 m).

Table I. AROME simulation periods selected on the basis of the ERA-Interim reanalysis.

Month	The combination that best represents the wind climate in the period 1989–2007				Most windy reference year*	Least windy reference year*
January	1991	1993	2000	2007	1989	2004
February	1989	1992	1998	2006	1989	1994
March	1991	1994	2002	2006	1997	2006
April	2000	2003	2005	2005	2007	2004
May	1991	1996	2000	2005	2000	1994
June	1989	1991	1992	1994	2000	1997
July	1992	2000	2002	2006	1999	1997
August	1994	1997	2001	2007	2005	2006
September	1991	1996	2003	2006	2005	1993
October	1995	1997	1998	1999	2005	1992
November	1992	1997	2004	2005	1999	2002
December	1989	1990	2000	2002	1992	2000

*The most windy reference year is a hypothetical year composed of the most windy months in the period 1989–2007. Analogously for the least windy reference year.

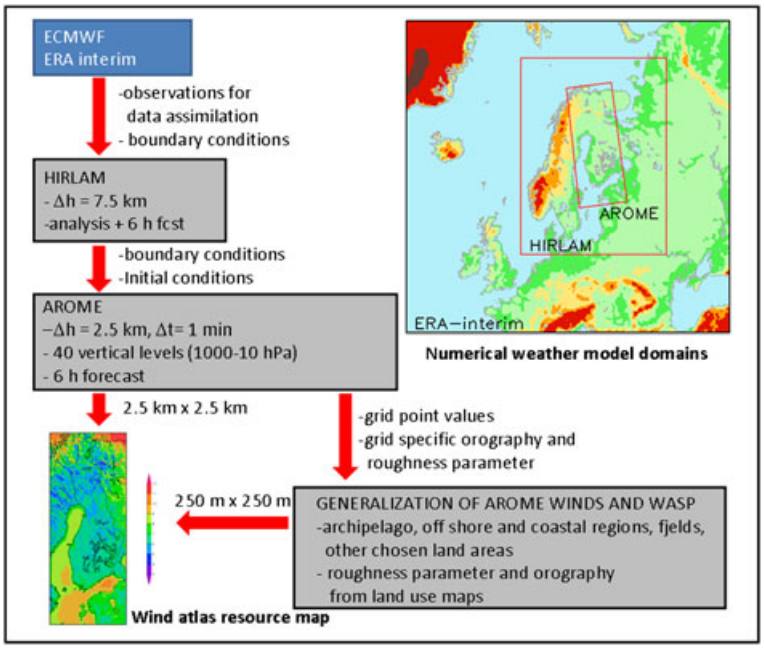

Figure 1. Modelling strategy for the Finnish Wind Atlas. Δh denotes the horizontal resolution and Δt is the model time step.

The initial state for the HIRLAM runs (and consequently for AROME) was produced by using both surface (2 m temperature and relative humidity, surface pressure, snow depth and sea surface temperature) and upper-air observations (TEMP/PILOT soundings and AMDAR aircraft observations, if available) within a variational data assimilation scheme. The data required at the edges of the HIRLAM domain were taken from the ERA-Interim reanalysis, which has an 80 km horizontal resolution. With the available computing resources, the modelling task was carried out in 8 months.

In the Finnish Wind Atlas, the AROME results are presented in a 2.5 km horizontal grid, and the data are linearly interpolated at eight levels above the Earth surface: 50, 75, 100, 125, 150, 200, 300 and 400 m.

2.3. Wind generalization and the use of WAsP

The AROME-based winds in the ABL strongly depend on the roughness length (z_0) and orography applied in the model. Because of the limited resolution, AROME presents a simplified version of the real terrain. To apply the modelled surface winds outside of the AROME framework, a so-called generalization process is needed. The process, developed at Risø DTU and applied in many wind atlas calculations,[8,13] standardizes the AROME surface winds providing hypothetical surface winds for a flat terrain with homogeneous roughness. Hence, the generalized surface winds no more depend on the z_0 and orography of AROME and can be applied utilizing the WAsP model together with more detailed information on the local terrain. WAsP[2] (see also www.wasp.dk) contains a suite of microscale models originally developed for prediction of wind resources over the area surrounding a meteorological station, taking into account the effects of local changes in roughness[14,15] and elevation.[16] An obstacle model is also included in WAsP but not used in this study. The following paragraphs describe how the generalization is performed on AROME winds.

The generalized wind climate comprises of profiles of sector-wise wind speed distributions given at a number of generalization heights (here 10, 25, 50, 100 and 200 m) for a set of generalization z_0 values (here 0.0002, 0.03, 0.1 0.4 and 1.5 m). In practice, the generalized winds were obtained using the AROME results for wind velocity (interpolated to the heights of 50, 100 and 200 m) and surface fluxes of momentum and heat, as well as AROME values for surface elevation and z_0. For the generalization heights of 10 and 25 m, the winds were calculated on the basis of the Monin–Obukhov similarity theory applying the AROME 50 m winds and the surface momentum and heat fluxes. For each of the generalization heights, a topographic correction was calculated using the linear flow model LINCOM.[17] The correction accounts for changes in wind speed due to changes in elevation (orographic speed up) and z_0. Once the generalization was performed for all simulations, wind speed distributions were fitted to the Weibull distribution.

The topographic corrections were applied to the interpolated winds at the generalization heights to provide winds over a flat terrain with homogeneous roughness. The homogeneous z_0 depends on the location and wind direction. To calculate

the winds for the generalized roughness lengths (independent of direction and location) at a specific generalization height z, neutral conditions and a logarithmic profile were assumed to solve u_* corresponding to the z_0 in AROME, and then the geostrophic wind speed V_g was calculated using the geostrophic drag law:

$$V_g = \frac{u_*}{\kappa}\sqrt{\left(\ln\left(\frac{u_*}{f\ z_0}\right) - A_G\right)^2 + B^2} \tag{4}$$

where f is the Coriolis parameter and A_G and B are empirical constants, here taken as 1.8 and 4.5, respectively, appropriate for neutral conditions. Then the geostrophic drag law was applied iteratively to solve for u_*, given V_g, for each of the generalization roughness lengths. Finally, the logarithmic profile was applied to give the wind speed at the generalization height in question. The procedure had to be carried out 25 times, for each of the five generalization roughness lengths and for each of the five generalization heights. At this point in the generalization process, the framework was neutral stratification. However, the wind at each generalization height was considered separately. Hence, the profile of generalized wind can depart from the logarithmic profile. This is indeed an advantage of the method, as the features of the wind profile in the mesoscale model are to some extent preserved.

The generalization calculations were made for all AROME output. Then the sector-wise distribution of the generalized winds was obtained. This distribution was partitioned into 12 direction sectors, and the Weibull distribution, with parameters A and k, was fitted to the wind speed distribution in each sector.

By using the principles of the generalization system, WAsP is typically used in the framework where the effects of the local orography and z_0 fields at the measurement site are first removed. In the Finnish Wind Atlas, however, the first step was to remove the effects of the orography and z_0 fields of AROME to calculate the monthly generalized wind climate. For each of the generalization heights and roughness lengths and for each sector, the histogram of the wind speed distribution was calculated, and a Weibull distribution was fitted. The generalized wind climates (WAsP LIB-files[2]), calculated for the 2.5×2.5 km^2 grids from the AROME results, were then given as input for WAsP, which were applied at selected areas at 250×250 m^2 horizontal resolution. The roughness maps applied in WAsP were made on the basis of Coordination of Information on the Environment land use data. In the roughness maps, the minimum size of a roughness area was 25 ha, and the minimum feature width was 100 m. For a smooth wind resource surface to be obtained, simple inverse-distance weighted interpolations between the three nearest AROME grid points were performed for every set of WAsP calculations.

If a user needs results at a resolution better than 250×250 m^2, these can be calculated by using the WAsP LIB-files or the AROME wind data from a suitable height as input wind climate for microscale modelling. An interpolation tool for LIB-files is included in WAsP version 10.

3. POST-PROCESSING OF AROME RESULTS

Here, we describe the calculation of the Weibull distribution parameters, gust factor, potential power production and power content, presented in the wind atlas with a 2.5 km resolution. The AROME results were first linearly interpolated to the wind atlas output heights, and the post-processing was made at these heights.

Following Garcia,[18] the scale (A) and shape (k) parameters of the Weibull distribution were calculated in each model grid point on the basis of the relative standard deviation of the wind speed distribution. A and k were calculated for all cases in each month and separately for stable, neutral and unstable stability classes. The stability criterion was chosen on the basis of the bulk-Richardson number, calculated on the basis of the potential temperature and wind speed differences between adjacent model levels. The following stability criteria were applied: stable, $Ri > 0.05$; near-neutral, $-0.15 \leq Ri \leq 0.05$; and unstable, $Ri < -0.15$. At the height of 50 m, averaged over Finland and the 48 month simulation period, the categories of stable, neutral and unstable stratification included 51%, 35% and 14% of the simulated cases, respectively. The Weibull A and k parameters were largest for neutral stratification and smallest for unstable stratification.

The method to calculate the gust factor was derived from Brasseur.[19] The original Brasseur method assumes that surface gusts result from deflection of air parcels flowing higher in the boundary layer and brought down by turbulent eddies. Instead of surface only, here we want to estimate the gust factor at several heights. For this purpose, the method was generalized assuming that the air parcel that can reach the surface should also be able to reach the levels above the surface. However, the mixing layer can be detached from the surface by a surface-based temperature inversion. In this case, the air parcel can only reach the levels above the inversion layer. The Brasseur method was first modified to define the mixing layer above each level individually. The second modification implemented is based on the fact that the turbulence transports momentum not only downward but also upward. Hence, a parcel flowing at some height below or above the level of interest

is able to reach the level, if the mean turbulent kinetic energy of large turbulent eddies is greater than the buoyant energy between the level of the air parcel and the level of interest. This can be formulated by the following pair of equations:

$$\frac{1}{z_l - z_p}\int_{Z_p}^{z_l} E\,\mathrm{d}z \geq \int_{Z_p}^{z_l} g\frac{\Delta\theta_v}{\theta_v}\mathrm{d}z \qquad \text{for } z_p < z_l$$

$$\frac{1}{z_p - z_l}\int_{Z_l}^{z_p} E\,\mathrm{d}z \geq \int_{Z_l}^{z_p} g\frac{\Delta\theta_v}{\theta_v}\mathrm{d}z \qquad \text{for } z_p \geq z_l \tag{5}$$

where z_l is the level of interest, z_p is the height of the air parcel and $\Delta\theta_v$ is the difference of virtual potential temperature over a given layer. AROME results for E were not available at the surface and were thus extrapolated using a cubic spline polynomial. Spline-based extrapolation was used as the turbulent kinetic energy profile near the surface is often non-linear. Following Brasseur,[19] the wind gust estimate was then chosen as the maximum wind speed for all parcels satisfying (5). The gust factor was calculated as the ratio of the wind gust estimate to the wind speed at the level of interest. The gust factor was calculated at each level at each 3 h of model simulations, after which the monthly and annual means were calculated.

Under unstable and neutral conditions, the wind gust profiles resulting from the original and generalized methods were not essentially different, but under stable stratification, they sometimes differed greatly. Above the stable surface layer the wind speed often strongly increased with height.

The potential power production for each month (in megawatt-hour) was calculated for three types of wind turbines: (i) WinWinD 1 MW with rotor diameter of 56 m, (ii) WinWinD 3 MW with rotor diameter of 90 m and (iii) REpower 5 MW with rotor diameter of 126 m (WinWinD and REpower are manufacturers). The calculation was made using a linear interpolation between the tabulated values of wind speed and corresponding values of power output indicated in the technical specifications for each turbine. For all three wind turbine types, the power production was calculated for all temperatures; for WinWinD 3 MW, additional calculations were made separately for temperatures less than −15°C and less than 17°C. The threshold of −15°C was chosen to identify power production under cold weather conditions (a general statement used against wind energy has been that there is not enough wind energy available during cold periods when the electricity demand is high). The threshold of 17°C corresponds to the heating power demand of buildings (S17).

The average wind energy flux density ($P = 1/2\ \rho\ V^3$, where ρ is the air density) or shortly the power content (in Watt per square meter) was calculated for the whole wind speed spectrum and separately for 4 to 25 m s^{-1}, which represents a typical range between cut-in and cut-off speeds for large wind turbines.

4. VALIDATION OF MODEL RESULTS

Wind measurements made in weather stations and high (50–300 m) masts were not used directly for production of the wind atlas, but they were used to validate the methodology used. This was based on verification of operational AROME runs and related WAsP calculations in 2008–2009.

4.1. AROME validation

4.1.1. Application of radar and rawinsonde observations.

The AROME 6 and 12 h wind forecasts were compared to weather radar and rawinsonde wind observations for the period of July 2008–May 2009. Rawinsonde wind observations are considered to be of high quality, but their spatial and temporal resolution is poor. Doppler weather radars, on the other hand, provide wind information with a high spatial and temporal resolution. The FMI radar network consists of eight Doppler weather radars that cover most of the country.[20]

The radar wind observations used in the validation have a 1000 m resolution in range, which corresponds to approximately 35 m resolution in height. In practice, however, the vertical resolution is decreased because the radar measurement volume increases with increasing measurement range from the radar. The validation makes use of an observation operator,[21] which produces the model counterpart for the observed quantity. The radar radial wind observation operator takes into account the broadening and bending of the radar pulse path.

The bias estimation method introduced in Salonen *et al.*[22] was applied. Figure 2 shows the wind speed bias and standard deviation calculated against rawinsonde observations, as well as the wind speed bias and the standard deviation of the radial wind component calculated against the radar observations. The period considered is September–November 2008. In both comparisons, the wind speed bias varied within ±0.6 m s^{-1} and the standard deviation varied from 2 to 3.5 m s^{-1}. Further details about the assessment are presented by Salonen *et al.*[23]

Figure 2. Locations of mast observations in southern Finland. The numbers correspond to the station numbers in Table II.

In general, the validation results indicated that the AROME wind forecasts are of good quality. The wind speed bias and standard deviation did not depend on the season. The number of radar observations used in the validation was approximately 4000 times larger than the number of rawinsonde observations. The large number of radar observations increases the statistical significance of the results. In conclusion, radar wind observations are a very useful source of independent observations to be used in wind forecast validation.

4.1.2. Application of mast observations.

The purpose of the validation was to estimate how well the model wind speed in a grid point corresponds to the observed wind speed at the mast. Because a mesoscale NWP model has been used to provide the detailed wind climate, the validation was made according to forecast verification framework.[24–26] The validation period was from the beginning of July 2008 to the end of July 2009. The measurement height was about 30 m at the sea and coastal areas and between 60 and 100 m in Helsinki Testbed masts (http://testbed.fmi.fi/index.html). More than 20 stations were available.

The wind speed of a grid point on a certain level corresponds to a mean value of a 2.5×2.5 km^2 square. Also, the model orography corresponds to a mean orography of the same area. In hilly areas, the difference between the model orography and real orography is sometimes significant. The interpolation of wind speed from model levels to constant height levels may also introduce error. Both model results and observations include errors; a quality control was performed to all data, and indistinct observations and outliers were excluded. The validation of wind speed was made separately to every available station to find out if there are differences in the error structure between masts in inland, near the coastline and in sea areas. The mean error (ME) and standard deviation of error (STDE) were calculated for all stations (Figure 3; Table II). The ME corresponds to the difference between model mean wind speed and observed mean wind speed if the data sample is the same. The comparison of results between different masts is not easy because the number of observations differed from station to station. Some masts had only 10% of all possible observations, whereas some Helsinki Testbed stations had more than 75%.

The results of the validation indicate that the error differs from mast to mast (Table II). The wind speed is overestimated at some stations and underestimated at others. At stations near coastline, the model seems to underestimate the wind speed more than in open sea or inland areas. Also, the day–night difference is large. The wind speed in the afternoon seemed to be too strong and in early morning hours too weak (not shown). The ME over all representative masts was calculated (Table II). The representativeness was estimated according to the number of observations and the level of STDE. If the number of available observations was 45% or less, or if the level of STDE was higher than 2.1, the mast was excluded from further calculations. Corresponding results from coastal SYNOP stations are shown in Table III. The SYNOP wind data were truly independent, since these were not used in the data assimilation procedure of the NWP models.

The results show that there is a small positive bias in AROME wind speed at levels 30–100 m. The mean positive bias is around 0.2–0.3 m s^{-1}. The level of STDE in masts and SYNOP stations is similar. The AROME model showed slightly better performance when the values of STDE were compared with the verification results of other operative NWP models at FMI.

4.2. Validation of the combined use of AROME and WAsP

For the combined AROME + WAsP method to be validated, the wind data produced by the operationally run AROME for the period of 1 June 2008 to 31 September 2009 were used as input data for WAsP. AROME winds at one altitude (80 or

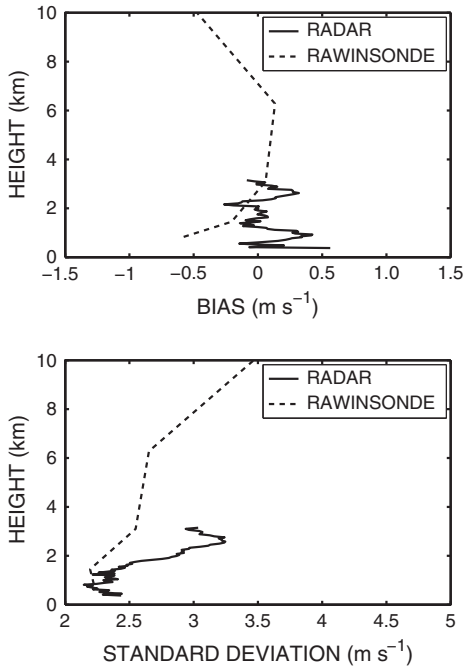

Figure 3. Wind speed bias (above) and standard deviation (below) as a function of height calculated against rawinsonde observations at Jyväskylä and radar observations at Vimpeli, both in central Finland. In the case of radar observations, the standard deviation is calculated for the radial wind component only. The period is September to November 2008.

Table II. Summary of comparison of AROME winds and mast observations over the period from 1 July 2008 to 31 July 2009.

Station	No	*H*	*N*	*A*	*O*	*ME*	*STDE*
Hanko	1	73	2535	7.8	6.9	0.9	(2.4)
Vänö	4	80	2496	8.4	8.3	**0.1**	1.8
Bågaskär	5	83	(1377)	8.6	8.9	−0.3	(2.2)
Padva	7	79	1935	7.4	7.1	0.3	(2.3)
Degerö	8	81	2128	7.3	6.2	**1.1**	1.8
Suvisaaristo	10	61	1854	6.8	5.9	**0.9**	1.9
Pirttisaari	12	61	(988)	9.2	8.4	0.8	1.8
Roihuvuori	15	100	2030	7.0	6.5	**0.6**	2.0
Oulunkylä	16	92	1499	6.6	6.6	−0.0	(2.9)
Essvik	19	86	2089	6.9	6.3	**0.6**	1.9
Boxby	20	80	(1047)	6.3	5.6	0.7	1.8
Luhtaanmäki	23	61	2203	4.7	5.2	**−0.5**	1.5
Monnikylä	27	80	(1481)	5.4	5.7	−0.3	1.6
Viirilä	28	81	2125	5.6	5.8	**−0.2**	1.5
Isosaari	36	83	1905	7.6	7.5	**0.1**	1.9
Isosaari	36	62	1905	7.3	7.1	0.2	1.9
Isosaari	36	42	1905	7.1	6.7	0.4	1.9
Mean value						**0.34**	

The explanation of columns: *H* = height (m); *N* = number of observations; *A* = AROME mean wind speed; *O* = observed mean wind speed; *ME* = mean error; *STDE* = standard deviation of error. Parentheses in column *N* indicate that the number is less than 45% of potential observations, and the station is therefore not included in the calculation of *ME*. Parentheses in column *STDE* also indicate that the station is excluded from the calculation of *ME* or error over stations. The stations included in the calculation of the station-averaged *ME* are marked by a bold number in the *ME* column.

100 m) at the grid point nearest to the measurement mast were used. Helsinki Testbed masts, FMI's other measurement masts and measurement masts of commercial companies were used in the validation. We were, however, not allowed to publish some of the commercial mast data.

Table IV shows the mean wind speeds on the basis of the mast measurements and the AROME + WAsP method for the entire validation period, and Table V presents the results for summer (from June to September) and winter (from November

Table III. Summary of comparison of AROME winds and SYNOP observations over the period from 1 July 2008 to 31 July 2009.

Station	*H*	*N*	*A*	*O*	*ME*	*STDE*
Helsinki lighthouse (WMO: 02989)	32	3033	7.8	7.4	0.4	1.9
Kalbådagrund (WMO: 02987)	32	3036	7.7	7.7	−0.0	1.9
Utö (WMO: 02981)	15/31	3028	7.9	7.1	0.8	1.9
Hanko (WMO: 02982)	27/40	3022	7.8	8.1	−0.3	2.0
Kemi I (WMO: 02863)	26	3014	7.1	7.0	0.1	1.9

The explanation of columns: *H* = height (m); *N* = number of observations; *A* = AROME mean wind speed; *O* = observed mean wind speed; *ME* = mean error; *STDE* = standard deviation of error.

Table IV. Validation of wind speeds based on the AROME + WAsP method for the period 1 June 2008 to 31 September 2009.

				Mean wind speed		
Observation site	Area	Observation height a.g.l (m)	Anemometer heating	Observations (m s^{-1})	Model (m s^{-1})	Difference (m s^{-1})
Vätingen	Åland	36	No	6.5	7.1	−0.6
Långnappan	Åland	45	No	5.3	5.5	−0.2
Isosaari	Archipelago	83	Yes	7.5	7.6	−0.1
	Archipelago	62	Yes	7.1	7.2	−0.1
	Archipelago	42	Yes	6.7	6.7	0
Bågaskär	Archipelago	27	Yes	6.1	6	0.1
Mäkiluoto	Archipelago	18	Yes	6.8	6.5	0.3
Vänö	Archipelago	80	Yes	8.3	8.3	0
Monninkylä	Inland	83	No	5.9	5.9	0
Viirilä	Inland	81	No	6.1	6.2	−0.1
Luhtaanmäki	Inland	61	No	5.3	5.3	0

Table V. As Table IV, but separately for summer and winter.

		Summer mean wind speed			Winter mean wind speed		
Observation site	Area	Observations (m s^{-1})	Model (m s^{-1})	Difference (m s^{-1})	Observations (m s^{-1})	Model (m s^{-1})	Difference (m s^{-1})
Vätingen	Åland	5.9	6.6	−0.7	6.9	7.5	−0.6
Långnappan	Åland	4.9	5	−0.1	5.5	5.8	−0.3
Torp	Åland	5.7	6.1	−0.4			
Degersand	Åland				6.6	6.3	0.3
Isosaari	Archipelago	6.8	7.2	−0.4	7.8	7.9	−0.1
	Archipelago	6.4	6.8	−0.4	7.5	7.6	−0.1
	Archipelago	6	6.4	−0.4	7.2	7.1	0.1
Bågaskär	Archipelago	5.7	5.6	0.1	6.4	6.5	−0.1
Mäkiluoto	Archipelago	6.1	6.2	−0.1	7.5	6.8	0.7

to March). There was very good agreement between the wind speeds predicted by the AROME + WAsP method and observations at Isosaari and Vänö islands. However, the difference between observations and the AROME + WAsP results varied between masts in the costal area and archipelago. The error was typically ± 0.3 m s^{-1}. At inland sites, the AROME + WAsP method worked very well; the error was approximately 1% only (Table IV).

5. CLIMATOLOGICAL ASPECTS

5.1. Fifty year maximum winds

The wind atlas represents the monthly and annual wind climate during the period 1989–2007, but users are also interested in the probability of extreme winds. Hence, the maximum wind speed for a 50 year return time (V_{50}) was calculated for each 2.5×2.5 km^2 grid cell at the heights of 10 and 100 m. The analysis was based on the 850 hPa level winds obtained from the ERA-40 data in the period 1958–2001. The method to downscale from 850 hPa level to 10 m above ground level was the same as in Kristensen *et al.*[27] and Mann *et al.*[28]: the geostrophic drag law (3) was applied, and V_{50} at the height of 10 m was calculated for a flat and homogeneous area with a z_0 of 0.05 m, which corresponds to engineering standards

for structural design. Calculating V_{50} for the height of 100 m, the real local z_0 was estimated for each 2.5×2.5 km^2 grid cell, using the Coordination of Information on the Environment land use data with 25 m resolution with an averaging function. A stepwise orographic height level correction function was implied to each V_{50} wind speed value; the correction was significant (up to 40%) for locations higher than 400 m a.s.l. A logarithmic profile was used to calculate the wind speed at 100 m.

Comparison of the extreme wind climate obtained from ERA-40 with the observed 50 year maximum wind at several Finnish weather stations is presented in more detail in Clausen *et al.*[29] At six of eight weather station sites, the predicted V_{50} was within the confidence limits of the Gumbell analysis on ERA-40 extreme wind data. At two sites, the ERA-40 extreme wind data clearly differed from the observed maximum wind, which was at least partly due to an inaccurate description of the local surroundings.

Using the real z_0, the highest V_{50} values at the height of 100 m were above 30 m s^{-1}, occurring in the sea areas, along the coasts, over a few larger lakes and over the northern fjelds (Figure 4; to produce the plot, the z_0 values of each grid cell were smoothed over a 10 km radius). The lowest V_{50} values were 18–22 m s^{-1}, found in the forested mainland. A few field areas in western Finland had maximum V_{50} values in the bin of 22–26 m s^{-1}.

5.2. Impact of climate change

Numerical simulations applying global climate models (GCMs) project significant changes in the occurrence and tracks of extratropical cyclones during this century.[30–33] For instance, Leckebusch and Ulbrich[31] using the Met Office Unified Model (HadCM3) and Bengtsson *et al.*[32] employing the Max Planck Institute coupled atmosphere–ocean model (ECHAM5) found that the storm track in the northernmost part of the Atlantic Ocean and the Norwegian Sea in winter will weaken until 2100, whereas in the region covering the British Isles and the area towards Scandinavia and Finland, there will be a distinct increase in the cyclone activity.

These findings motivated us to explore the impact of climate change on winds in Finland. The surface geostrophic wind speeds in Finland have been investigated by employing nine GCMs (BCCR-BCM2.0, CGCM3.1 (T63), CNRM-CM3, ECHAM5/MPI.OM, GFDL-CM2.1, IPSL-CM4, MIROC3.2 (hires), MRI-CGCM2.3.2, NCAR-CCSM3) forced by three Special Report on Emission Scenarios[34] greenhouse gas scenarios. Among these scenarios, the A2 scenario represents a pessimistic future with the atmospheric carbon dioxide concentration increasing up to about 840 ppm by 2100. In the optimistic B1 scenario, the corresponding concentration is approximately 540 ppm, and in the intermediate A1B scenario, it is

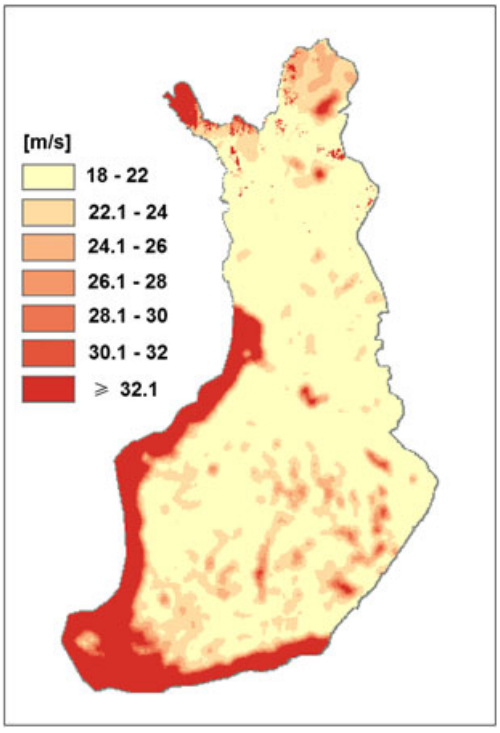

Figure 4. Spatial distribution of the 50 year maximum wind at the height of 100 m.

700 ppm. Simulations with the A1B scenario were available for all the nine models, A2 for seven models, and B1 for eight models. The grid size of the individual models varied from 100 to 300 km. The periods studied were 1971–2000, 2046–2065 and 2081–2100. The surface geostrophic wind speeds were deduced from the simulated sea level pressure fields; for details, see Gregow *et al.*[35] By comparing the model-inferred geostrophic winds with the corresponding observation-based (ERA-40) estimates, the observed monthly mean wind speeds were found to differ from the multimodel mean by less than one standard deviation of the modelled changes.

Inside the boundaries of Finland, no statistically significant changes in the mean surface geostrophic wind speeds were found until 2046–2065 compared with the baseline period 1971–2000. By the end of the century (2081–2100), there is an increase of 2% to 4% in the September to April mean in southern Finland according to the A1B and A2 scenarios. Even larger increases are projected for the southern Baltic Sea. The response to the B1 forcing is weaker and statistically less significant, but the patterns of change are qualitatively similar for all three scenarios. Changes in the extreme winds on the 10 and 50 year return level are of the similar order of magnitude, but the largest increases are concentrated on northern Finland and north-western Russia.

On the basis of Gregow *et al.*,[35] the monthly mean changes can be even larger. The time-mean surface geostrophic wind speeds were projected to strengthen most in October to February. Especially November seems to become windier: by the end of the century, according to the model ensemble, the increase is 5% to 10%. However, the scatter among the model simulations is quite large, ranging from -5% to approximately $+15\%$. In summer, the mean geostrophic wind speeds generally manifest no statistically significant change.

6. RESULTS OF THE WIND ATLAS

The wind atlas data are disseminated through the dynamic wind atlas maps, available at www.windatlas.fi. The map system is built on top of an open-source Mapserver map engine, originally developed in the University of Minnesota. The web user interface is a modified version of an open-source Ka-Map JavaScript package. The total amount of the Finnish Wind Atlas data is about 60 GB, which is stored into PostgreSQL/Postgis database. There are 130 different data layers for a user to view on top of some basic geographic layers. When a user is browsing data, visualization is carried out on the fly, and created map tiles are stored on disk cache to speed up following similar requests for the same map area. A user can also make data requests from database by selecting an area from the map, and the user obtains data in a table format for a spreadsheet application or in WAsP LIB-file format.

We may expect that the spatial distribution of near-surface wind speed is controlled by the distributions of the geostrophic wind speed, orography, roughness and stratification. As examples of the wind atlas results, in Figures 5 and 6 we present the distributions of these variables (using wind at the 850 hPa level as an estimate of the geostrophic wind) in May and December, which represent the opposite months from the point of view of land–sea temperature difference (the constant orography and almost constant roughness are only shown for December). We see that the monthly mean wind speed at the height of 100 m (V_{100} m) is strongly controlled by z_0 (Figure 5(b)) with strongest winds over the sea and, to some extent, lakes in the eastern Finland (Figure 6(a), (b)). In northernmost Finland, the local maxima in V_{100} m are due to combined effects of higher orography and reduced roughness. In December, the stratification is most unstable over the sea (Figure 5(d)), which enhances the maximum in V_{100} m (Figure 6(b)). In May, the stratification is stable over the sea and lakes but unstable over most land areas (Figure 5(c)), which reduces the sea–land difference in the wind speed close to the surface (not shown) but the effect is no more evident at the height of 100 m (compare Figures 6(a), (b)). Compared with V_{100} m, the effects of roughness and stratification are amplified in the distribution of potential power production at the height of 100 m (Figure 6(c), (d); calculated for WinWinD 3 MW turbine). Spatial variations in the geostrophic wind speed are minor (Figure 5(c), (d)) without detectable effects on V_{100} m and the power production.

7. DISCUSSION AND CONCLUSIONS

The production of the Finnish Wind Atlas represents a new approach to analyse wind and wind energy climate. The AROME model was run with a 2.5 km horizontal resolution for a total of 72 months. The amount of mesoscale model runs was accordingly much larger than made for any other wind atlas (see Section 1). In any case, the wind atlas could not have been produced solely on the basis of AROME: if a horizontal resolution of 250 m instead of 2.5 km were used in AROME, the model runs with the same amount of computing resources would have taken more than 600 years instead of 8 months. Hence, the wind generalization and application of WAsP was essential. It required a new strategy for the use of WAsP. Instead of giving local wind observations from masts as input for WAsP, AROME winds were applied. They represent grid-averaged results and accordingly the roughness lengths applied in AROME grid cells had to be taken into account in the wind generalization. The development of this new strategy opens possibilities for wider applications of WAsP.

Compared with previous national wind atlases, a new approach in the Finnish Wind Atlas was that the results were calculated separately for each month and for sectors 30° wide. The sector-specific wind climatology is essential for coastal

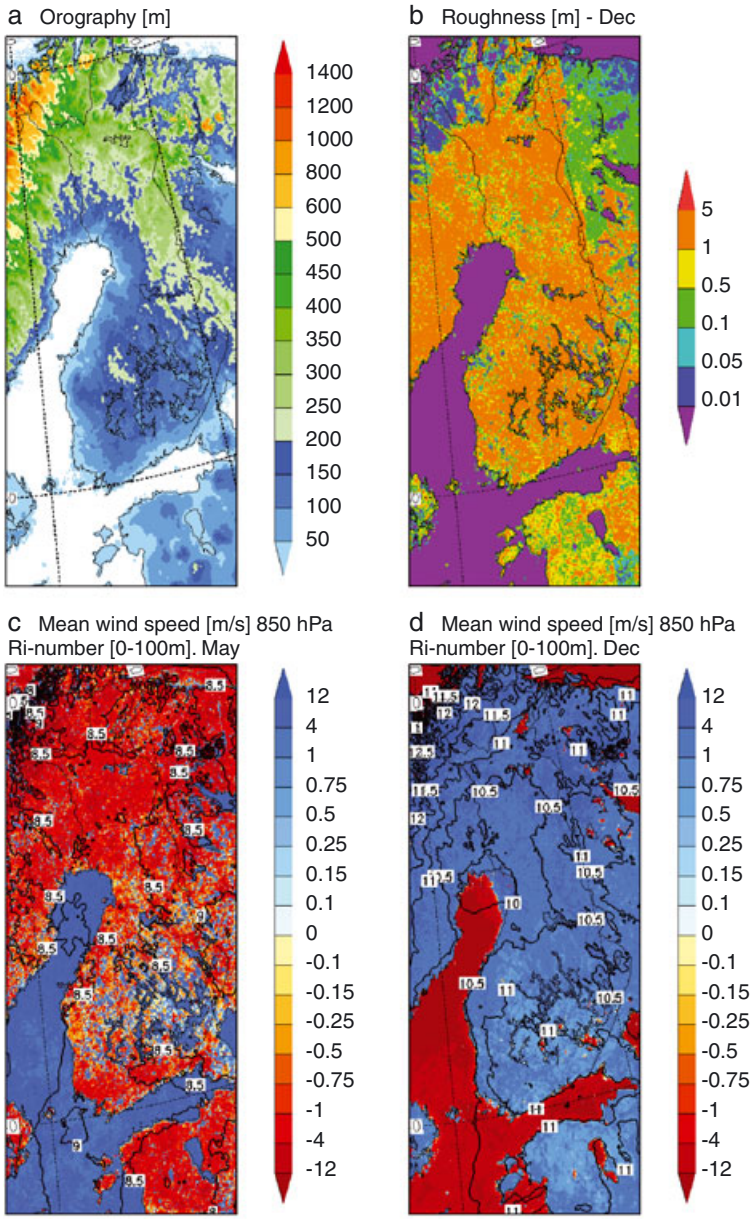

Figure 5. Spatial distributions of (a) orography, (b) aerodynamic roughness length, as well as the monthly mean Richardson number (colour scale) and 850 hPa wind speed (isolines with numbers) in (c) May and (d) December.

regions, and the monthly division is particularly important in high latitudes, where the seasonal changes in ABL stratification are large. Over the Baltic Sea, the ABL stratification is usually stable during spring, near-neutral during summer,[36] unstable during autumn and stable over sea ice but unstable over the open sea in winter.[37] Sea ice usually has a larger z_0 than the open sea, but the stratification effect is even more important for the wind speed.[38] Over the mainland, the roughness varies depending on the state of vegetation and presence of snow cover. The latter also strongly affects the ABL stratification. Under the same pressure gradient, the near-surface winds are stronger under unstable than stable ABL stratification, but stable stratification favours the generation of low-level jets.[4]

To demonstrate the magnitude of inter-annual variability, we also included in the Finnish Wind Atlas statistics for the windiest and calmest months in the period of 1989–2007. Climate models cannot reliably predict the inter-annual and decadal variability. The climate change in the time scale of 50–100 years is, however, more predictable, and we have analysed GCM projections for the changes in the surface geostrophic wind during this century. The models predict an increase

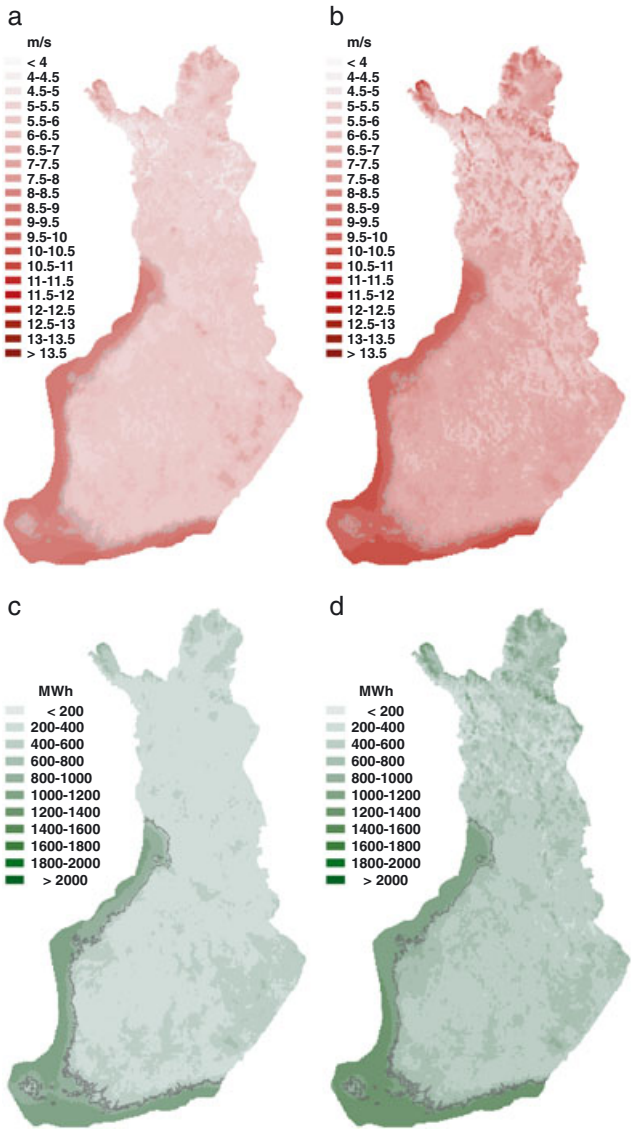

Figure 6. Spatial distributions of the wind speed at the height of 100 m in (a) May and (b) December and the potential power production for the WinWind 3 MW turbine for (c) May and (d) December.

of 2–4% in the annual mean geostrophic wind by the end of the century. The relationship between the geostrophic wind and the true wind speed in the ABL depends, however, on the roughness and stratification. Hence, via changes in wintertime ABL stratification, the expected reduction of sea-ice cover[39] may have even larger effects on the true wind speed than changes in the geostrophic wind.

We used an extensive set of coastal, archipelago and lighthouse stations for the wind atlas validation. Validation of model predictions for wind speed at heights up to 400 m is a challenge, and only a small number of point measurements have usually been available for that. The application of Doppler weather radar winds in the AROME validation was a novel aspect in the Finnish Wind Atlas. The number of radar observations used in the validation was approximately 4000 times larger than the number of rawinsonde observations, strongly increasing the statistical significance of the results. Moreover, radar winds provided independent observations for the validation. Using new methods to derive the wind speed (instead of the radial wind component only) from the radar data,[22,23] a satisfactory accuracy of the AROME results (bias within ± 0.6 m s^{-1}) was found.

In addition to the results directly based on AROME and WAsP, we included in the wind atlas several quantities based on post-processing of the model results: the Weibull distribution parameters, gust factor, potential power production and

power content. The parameterization of the gust factor was based on a novel approach because the existing parameterization methods were not directly applicable for heights up to 400 m.

Wind conditions over fjelds still represent a challenge, both for modelling and representativeness of observations.[40] We did not have much data for validation of the results over fjelds. Further efforts are accordingly needed in this field. An issue not included in the Finnish Wind Atlas is the ice accretion in wind power plants.[41] This is addressed in an ongoing study.

Disseminating and distributing the wind atlas data with visual and freely zoomable webservice allows users to select data for viewing and downloading from the area they are interested. Compared with static images from fixed areas, this is novel and flexible approach allowing large data downloads from a file transfer protocol server. It is also possible to obtain the data through a Web Map Service protocol. In addition to applications related to wind power production, the wind atlas has also been used in planning of land use.

As a summary, the methodology applied in the Finnish Wind Atlas included the following novel aspects: (i) a climatologically representative period of 48 months was simulated with the mesoscale model; (ii) in addition, the windiest and calmest months during the period of 1989–2007 were simulated; (iii) the results were calculated separately for each month and for sectors 30° wide; (iv) instead of point measurements, the WAsP calculations were based on the mesoscale model outputs; (v) in addition to point measurements, also radar wind data were applied for the validation of the mesoscale model results; (vi) the parameterization method for the gust factor was extended to account for gusts at the heights up to 400 m; and (vii) the dissemination of the wind atlas was based on new technical solutions.

ACKNOWLEDGEMENTS

The production of the Finnish Wind Atlas was supported by the Ministry of Labour and Economics. We thank the four anonymous reviewers for their fruitful comments that helped to improve the manuscript.

APPENDIX A. AROME MODEL

AROME[42] is a non-hydrostatic spectral model of which the dynamical core is based on a two-time-level semi-implicit semi-Lagrangian discretization of the fully compressible Euler equations.[43] The model uses a mass-based terrain-following hybrid coordinate system in the vertical. In the frame of its horizontal and vertical resolution, the AROME model can resolve and thus treat explicitly motion systems down to the scale of 4–6 times the grid spacing (in this application about 10–15 km). A variety of subgrid-scale physical processes are taken into account by parameterization schemes. Here, we briefly summarize the schemes that most directly affect the results of the wind atlas: the surface, ABL and shallow convection schemes.

In AROME, the subgrid scale vertical flux F_S of a resolved variable S is expressed as

$$F_S = K_S \, \partial S/\partial z + M(S_U - S) \tag{A1}$$

where the first term on the right-hand side represents small-scale turbulence and the second term accounts for the vertical transport by shallow convection. Here, K_S is a turbulent diffusivity for the property S, M is an effective updraft velocity and S_U stands for the value of S in the updrafts. The diffusive part is parameterized according to Cuxart *et al.*[44] K_S depends on a mixing length, diagnosed non-locally from the (prognostic) turbulent kinetic energy and static stability, as described by Bougeault and Lacarrère.[45] The contribution of shallow, non-precipitating cumulus convection and dry thermal (second term on the right-hand side of (1)) is parameterized in terms of the vertical mass flux and properties in the convective updrafts.

The turbulent surface fluxes of momentum, heat and moisture are parameterized by the surface module SURFEX,[46] which applies the Monin–Obukhov theory with stability-dependent exchange coefficients. Subgrid-scale surface heterogeneities are treated using a tiling approach, where surface characteristics, such as the aerodynamic roughness length z_0, and stability functions depend on the tile. Four surface tiles are allowed in each model grid box: nature, town, sea and lake. The sea and lakes may be frozen, and nature and town may be covered by snow, which is described by a prognostic snow scheme. The nature tile is treated according to the Interaction Soil-Biosphere-Atmosphere formulation[47,48] with up to 12 vegetation types, each having their own z_0 and other physical characteristics. These are then used to calculate surface fluxes for each tile. For the whole grid, the fluxes are calculated as area averages. So, the atmosphere is sensing only the grid-averaged fluxes. In most of the 12 vegetation types z_0 depends on the leaf-area index (LAI) and height of trees (HT). LAI is a climatological value and chances during the year, whereas the HT is constant in time but depends on the latitude. The most essential nature tiles in Finland are deciduous broad-leaved and needle-leaved forests. The z_0 for vegetation is calculated as follows:[49]

$$z_0 = \max(0.001, z_{\mathrm{ref}} \times \exp(-1/\sqrt{z_{\mathrm{sum}}})) \tag{A2}$$

Table AI. Vegetation height z_i applied in AROME.

Vegetation type	z_i (m)
Crops	Min(2.5,exp((LAI-3.5)/1.3)
Irrigated crops	Min(2.5,exp((LAI-3.5)/1.3)
Broadleaf forest	HT
Coniferous forest	HT
Grassland	LAI/6
Irrigated parks	LAI/6
Bare ground	0.1
Permanent snow	0.01
Rocks	1

HT is the height of trees in metres and LAI is the leaf-area index.

where

$$z_{\text{sum}} = \sum_i \frac{f_i}{(\ln(0.13 \times z_i / z_{\text{ref}}))^2} \tag{A3}$$

where z_{ref} is a reference height of 10 m and z_i is a height of vegetation as given in Table AI. f_i stands for the fraction of a vegetation type i. Values of LAI and HT are described in the ECOCLIMAP global database having a spatial resolution of 1 km.[50] In Finland, the HT in ECOCLIMAP varies from 10 to 15 m, which results in z_0 ranging from 1.3 to 1.95 m.

The surface temperature of the sea and lake tiles remain constant during the forecast, the spatially variable values being set in the initial conditions, obtained as described in Section 2.2. In the present application, the sea surface temperatures are based on actual data, whereas the lake temperatures represent climatological conditions. The Charnock[51] formula is used for calculating roughnesses for the sea and lake:

$$z_{0\text{sea}} = 0.015 \frac{u_*^2}{g} \tag{A4}$$

For ice-covered sea/lake, the roughness is constant: $z_{0\text{ice}} = 10^{-3}$ m. The sea or lake is assumed to be ice-covered when the surface temperature is less than −2°C. The town tile is based on the Town Energy Budget scheme.[26] Physiographic data for land surfaces are obtained from ECOCLIMAP. AROME includes nine different town types, but only one of these exists in Finland: this suburban town type has a constant roughness: $z_{0\text{town}} = 1$ m.

REFERENCES

1. Tammelin B. *Suomen Tuuliatlas—Finnish Wind Atlas (In Finnish with a resumee in English)*. Finnish Meteorological Institute: Helsinki, 1991; 356.
2. Mortensen NG, Heathfield DN, Rathmann O, Nielsen M. *Wind Atlas Analysis and Application Program: WAsP 10 Help Facility*. Risø National Laboratory for Sustainable Energy: Technical University of Denmark, Roskilde, Denmark, 2009; 356 topics.
3. Troen I, Petersen EL. *European Wind Atlas*. Risø National Laboratory: Roskilde, 1989; 656.
4. Högström U, Smedman AS. The wind regime in coastal areas with special reference to results obtained from Swedish Wind Energy Program. *Boundary Layer Meteorol* 1984; **30**: 351–373.
5. Bergström H, Söderberg S. Wind mapping in Sweden—summary of results and methods used. *Elforsk rapport* 2008; **09**: 04.
6. Costa P, Miranda P, Estanqueiro A. Development and validation of the Portuguese Wind Atlas. *Proceedings of European Wind Energy Conference*, Athens, Greece, 2006; 9.
7. Gastrón M, Pascal E, Frías L, Martí I, Irigoyen U, Cantero E, Loxano S, Loureiro Y. Wind resources map of Spain at mesoscale. Methodology and validation. *Proceedings of European Wind Energy Conference*, Brussels, Belgium, 2008; 10.
8. Frank HP, Rathmann O, Mortensen NG, Landberg L. The numerical wind atlas—the KAMM/WAsP method. *Risø-R-1252(EN)*, 2001; 60. [Online]. Available: http://130.226.56.153/rispubl/VEA/veapdf/ris-r-1252.pdf. (Accessed 5 September 2011)

9. Mortensen NG, Hansen JC, Badger J, Jørgensen BH, Hasager CB, Georgy Youssef L, Said Said U, Abd El-Salam Moussa A, Akmal Mahmoud M, El Sayed Yousef A, Mahmoud Awad A, Abd-El Raheem Ahmed M, Sayed MAM, Hussein Korany M, Abd-El Baky Tarad M. *Wind Atlas for Egypt, Measurements and Modelling 1991–2005*. New and Renewable Energy Authority, Egyptian Meteorological Authority and Risø National Laboratory, 2005; 258.
10. Sustainable Energy Ireland. Republic of Ireland—Wind Atlas 2003. *Project Report No. 4Y103A-1-R1*, 2003; 52. Available: http://www.seai.ie/uploadedfiles/RenewableEnergy/IrelandWindAtlas2003.pdf. (Accessed 5 September 2011)
11. Botta G, Casale C, Lembo E, Maran S, Serri L, Stella G, Viani S, Burlando M, Cassola F, Villa L, Ratto CF, The Italian Wind Atlas—status and progress. *Proceedings of European Wind Energy Conference 2007*, EWEA, Brussels, Belgium, 2007; 7.
12. Undén P, 26 co-authors. *HIRLAM-5 Scientic Documentation*. Swedish Meteorological and Hydrological Institute: Norrköping, Sweden, 2002; 144. [Online]. Available: http://hirlam.org/publications/SciDoc_Dec2002.pdf. (Accessed 5 September 2011)
13. Nygaard I, Rasmussen K, Badger J, Nielsen TT, Hansen LB, Stisen S, Larsen S, Mariko A, Togola I. Using modeling, satellite images and existing global datasets for rapid preliminary assessments of renewable energy resources: the case of Mali. *Renewable & Sustainable Energy Reviews* 2010; **14**: 2359–2371.
14. Sempreviva AM, Larsen SE, Mortensen NG, Troen I. Response of neutral boundary layers to changes of roughness. *Boundary-Layer Meteorology* 1990; **50**: 205–225.
15. Rao KS, Wyngaard JC, Coté DR. The structure of the two-dimensional internal boundary layer over a sudden change of surface roughness. *Journal of the Atmospheric Sciences* 1974; **26**: 432–440.
16. Jackson PS, Hunt JCR. Turbulent wind flow over a low hill. *Quarterly Journal of the Royal Meteorological Society* 1975; **101**: 929–955.
17. Astrup P, Jensen NO, Mikkelsen T. Surface roughness model for LINCOM. *Risø-R-900(EN)*, 1996; 30. [Online]. Available: http://130.226.56.153/rispubl/VEA/veapdf/ris-r-900.pdf. (Accessed 5 September 2011)
18. Garcia O. Simplified method of moments estimation for the Weibull distribution. *New Zealand Journal of Forestry Science* 1981; **11**: 304–306.
19. Brasseur O. Development and application of a physical approach to estimating wind gusts. *Monthly Weather Review* 2001; **129**: 5–25.
20. Saltikoff E, Huuskonen A, Hohti H, Koistinen J, Järvinen H. Quality assurance in the FMI Doppler weather radar network. *Boreal Environment Research* 2010; **15**: 579–594.
21. Järvinen H, Salonen K, Lindskog M, Huuskonen A, Niemelä S, Eresmaa R. Doppler radar radial winds in HIRLAM. Part I: observation modelling and validation. *Tellus* 2009; **61A**: 278–287.
22. Salonen K, Järvinen H, Eresmaa R, Niemelä S. Bias estimation of Doppler-radar radial-wind observations. *Quarterly Journal of the Royal Meteorological Society* 2007; **133**: 1501–1507.
23. Salonen K, Niemelä S, Fortelius C. Application of radar wind observations for low level NWP wind forecast validation. *Journal of Applied Meteorology and Climatology* 2011. DOI: 10.1175/2010JAMC2652.1, (to appear in print).
24. Wilks DS. *Statistical methods in the atmospheric sciences*. Academic Press: San Diego, USA, 1995; 467.
25. Jolliffe IT, Stephenson DN. *Forecast Verification: A Practitioner's Guide in Atmospheric Sciences*. Wiley: Chichester, UK, 2003; 240.
26. Nurmi P. Recommendations on the verification of local weather forecasts. *ECMWF Technical Memorandum 430*, Reading, UK, 2003; 19.
27. Kristensen L, Jensen G. Geostrophic winds in Denmark: a preliminary study. *Technical Report No Risø-R-1145*, Risø National Laboratory, Roskilde, Denmark, 1999.
28. Mann J, Ott S, Hoffman Jørgensen B, Frank HP. WasP Engineering. *Technical Report No Risø-R-1356*, Risø National Laboratory, Roskilde, 2002.
29. Clausen NE, Pryor SC, Guo Larsén X, Hyvönen R, Venäläinen A, Suvilampi E, Kjellström E, Barthelmie R. Are we facing increasing extreme winds in the future? *Proceedings of the European Wind Energy Conference and Exhibition, Marseille, France*, 16–19 March, 2009; 10. [Online]. Available: http://orbit.dtu.dk/Home.html. (Accessed 5 September 2011)
30. Carnell RE, Senior CA, Mitchell JFB. An assessment of measures of storminess: simulated changes in northern hemisphere winter due to increasing CO_2. *Climate Dynamics* 1996; **12**: 467–476.
31. Leckebusch GC, Ulbrich U. On the relationship between cyclones and extreme windstorm events over Europe under climate change. *Global and Planetary Change* 2004; **44**: 181–193.

32. Bengtsson L, Hodges KI, Rockner E, Storm tracks and climate change. *Journal of Climate* 2006; **19**: 3518–3543.
33. Leckebusch GC, Donat M, Ulbrich U, Pinto JG. Mid-latitude cyclones and storms in an ensemble of European AOGCMs under ACC. *Clivar Exchanges* 2008; **13**(3): 3–15.
34. Nakićenović N, 27 co-authors. *IPCC Special report on emission scenarios*. Cambridge University Press: New York, 2000; 599.
35. Gregow H, Ruosteenoja K, Pimenoff N, Jylhä K. Changes in the mean and extreme geostrophic wind speeds in Northern Europe until 2100 based on nine global climate models. *International Journal of Climatology* 2011. in press (JOC-10-0425.R1).
36. Niros A, Vihma T, Launiainen J. Marine meteorological conditions and air-sea exchange processes over the Baltic Sea in 1990s. *Geophysica* 2002; **38**: 59–87.
37. Vihma T, Haapala J. Geophysics of sea ice in the Baltic Sea—a review. *Progress in Oceanography* 2009; **80**: 129–148. DOI: 10.1016/j.pocean.2009.02.002.
38. Vihma T. Subgrid parameterization of surface heat and momentum fluxes over polar oceans. *Journal of Geophysical Research* 1995; **100**: 22,625–22,646.
39. Meier HEM. Baltic Sea climate in the late twenty-first century: a dynamical downscaling approach using two global models and two emission scenarios. *Climate Dynamics* 2006; **27**: 39–68. DOI: 10.1007/s00382-006-0124-x.
40. Tammelin B, Hyvönen R, Peltomaa A. The accuracy of wind measurements in hilly regions. In *Proceedings of BOREAS III, 19-21 March 1996, Saariselkä, Finland*, Tammelin B, et al. (eds). Finnish Meteorological Institute: Helsinki, 1996; 232–244.
41. Tammelin B, Cavaliere M, Holttinen H, Morgan C, Seifert H, Säntti K. *Wind Energy Production in Cold Climate*, Meteorological Publications, Vol. 41. Finnish Meteorological Institute: Helsinki, 2000.
42. Seity Y, Brousseau P, Malardel S, Hello G, Bénard P, Bouttier F, Lac C, Masson V. The AROME-France convective scale operational model. *Monthly Weather Review* 2011; **139**: 976–991. DOI: 10.1175/2010MWR3425.1.
43. Bénard P, Vivoda J, Masek J, Smolikova P, Yessad K, Smith C, Brozkova R, Geleyn JF. Dynamical kernel of the Aladin-NH spectral limited-area model: revised formulation and sensitivity experiments. *Quarterly Journal of the Royal Meteorological Society* 2010; **136**: 155–169.
44. Cuxart J, Bougeault P, Redelsperger JL. A turbulence scheme allowing for mesoscale and large eddy simulations. *Quarterly Journal of the Royal Meteorological Society* 2000; **126**: 1–30.
45. Bougeault P, Lacarrère P. Parameterization of orography-induced turbulence in a meso-beta-scale model. *Monthly Weather Review* 1989; **117**: 1872–1890.
46. Le Moigne P. SURFEX scientific documentation, 2009. [Online]. Available: http://www.cnrm.meteo.fr/surfex/doc_exter/surfex_scidoc.pdf. (Accessed 5 September 2011)
47. Noilhan J, Planton S. A simple parameterization of land surface processes for meteorological models. *Monthly Weather Review* 1989; **117**: 536–549.
48. Noilhan J, Mahfouf JF. The ISBA land surface parameterization scheme. *Global and Planetary Change* 1996; **13**: 145–159.
49. Le Moigne P. SURFEX setup, 2006. [Online]. Available: http://www.cnrm.meteo.fr/surfex/doc_exter/setup.pdf. (Accessed 5 September 2011)
50. Champeaux JL, Masson V, Chauvin R. Ecoclimap: a global database of land surface parameters at 1 km resolution. *Meteorological Applications* 2005; **12**: 29–32.
51. Charnock H. Wind stress on a water surface. *Quarterly Journal of the Royal Meteorological Society* 1955; **81**: 639–640.